ACS NANO

Cite This: ACS Nano 2018, 12, 8350–8361

www.acsnano.org

ARTICLE

Size-Dependent Band-Gap and Molar Absorption Coefficients of Colloidal $CuInS_2$ Quantum Dots

Chenghui Xia,[†,‡] Weiwei Wu,[†] Ting Yu,[†] Xiaobin Xie,[§] Christina van Oversteeg,[†] Hans C. Gerritsen,[‡] and Celso de Mello Donega*[,†]

[†]Condensed Matter and Interfaces, Debye Institute for Nanomaterials Science, Utrecht University, 3508 TA Utrecht, The Netherlands

[‡]Molecular Biophysics, Debye Institute for Nanomaterials Science, Utrecht University, 3508 TA Utrecht, The Netherlands

[§]Soft Condensed Matter, Debye Institute for Nanomaterials Science, Utrecht University, 3508 TA Utrecht, The Netherlands

S *Supporting Information*

ABSTRACT: **The knowledge of the quantum dot (QD) concentration in a colloidal suspension and the quantitative understanding of the size-dependence of the band gap of QDs are of crucial importance from both applied and fundamental viewpoints. In this work, we investigate the size-dependence of the optical properties of nearly spherical wurtzite (wz) $CuInS_2$ (CIS) QDs in the 2.7 to 6.1 nm diameter range (polydispersity ≤10%). The QDs are synthesized by partial Cu^+ for In^{3+} cation exchange in template $Cu_{2-x}S$ nanocrystals, which yields CIS QDs with very small composition variations (In/Cu = 0.91 ± 0.11), regardless of their sizes. These well-defined QDs are used to investigate the size-dependence of the band gap of wz CIS QDs. A sizing curve is also constructed for chalcopyrite CIS QDs by collecting and reanalyzing literature data. We observe that both sizing curves follow primarily a $1/d$ dependence. Moreover, the molar absorption coefficients and the absorption cross-section per CIS formula unit, both at 3.1 eV and at the band gap, are analyzed. The results demonstrate that the molar absorption coefficients of CIS QDs follow a power law at the first exciton transition energy ($\varepsilon_{E_1} = 5208d^{2.45}$) and scale with the QD volume at 3.1 eV. This latter observation implies that the absorption cross-section per unit cell at 3.1 eV is size-independent and therefore can be estimated from bulk optical constants. These results also demonstrate that the molar absorption coefficients at 3.1 eV are more reliable for analytical purposes, since they are less sensitive to size and shape dispersion.**

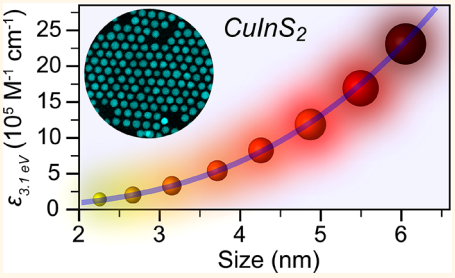

KEYWORDS: *copper indium sulfide, cation exchange, molar extinction coefficient, absorption cross-section, size-dependence*

Colloidal semiconductor quantum dots (QDs) exhibit size-dependent optoelectronic properties, making them promising materials for many applications, such as solution-processed solar cells,[1−3] luminescent solar concentrators,[1] photodetectors,[4] light-emitting devices,[1,5] optoelectronic devices,[1,6] and biomedical imaging.[7−9] The successful development of these applications requires a precise control over both the size and the concentration of the QDs. Additionally, an accurate knowledge of the QD concentration is also crucial for the synthesis of heteronanocrystals (*e.g.*, core/shell QDs),[10−12] preparation of QD superlattices,[13−15] and fundamental studies of the nucleation and growth of nanoparticles.[16] This has made the determination of the molar absorption coefficients ε of QDs an important endeavor, since optical absorption spectroscopy offers a very fast and convenient way to establish the concentration of colloidal suspensions of QDs. Moreover, the absorption cross-section of QDs is a relevant parameter for applications requiring the precise knowledge of the relationship between excitation fluence and exciton density per QD (*e.g.*, lasers). The quantitative understanding of the size-dependence of the optical properties of QDs also allows the construction of empirical sizing curves correlating the lowest energy absorption peak with the QD size, which can in turn be used to verify the validity of theoretical models describing quantum confinement effects and the nature of the radiative recombination in semiconductor nanocrystals. Nevertheless, the quantitative study of the size-dependence of the optical properties of QDs has been to date primarily focused on binary

Received: May 15, 2018
Accepted: August 7, 2018
Published: August 7, 2018

DOI: 10.1021/acsnano.8b03641
ACS Nano 2018, 12, 8350–8361

compositions (Cd-, Pb-, and Ag-chalcogenides,[17−35] InP,[36] and InAs[37,38]).

Ternary $CuInS_2$ (CIS) QDs have attracted increasing attention due to their nontoxicity, large absorption coefficients across a broad spectral range, and wide photoluminescence (PL) tunability through the visible to the NIR spectral window.[39−41] These QDs have been applied in light-emitting devices,[42−44] luminescent solar concentrators,[45−48] and biolabels.[49,50] However, despite the importance of these nanomaterials, there are at present only two reports on the size-dependence of the molar absorption coefficients of CIS QDs.[51,52] Intriguingly, the size dependence of the ε values at the first exciton transition energy (E_1) reported in these works is dramatically different: Qin *et al.*[51] reported a power law with an exponent of 2.1, while Booth *et al.*[52] found a power law with an exponent of 3.7. The latter work also reports that the ε values at higher energy (3.1 eV) scale with the diameter to the power of 3.8,[52] which is far stronger than the cubic size dependence that is theoretically expected, and has been experimentally observed in several binary chalcogenides.[23,25,28,34,38] Although the reasons for these discrepancies are as yet unclear, they may be attributed to the inherent difficulties associated with the determination of sizes, absorption peak positions, and concentrations of colloidal QDs. These experimental intricacies have in the past been responsible for large inconsistencies between results reported by different groups for the size-dependencies of the molar absorption coefficients and band gap of binary QDs, such as the prototypical CdSe.[24,25,27,29,31−33] From this viewpoint, CIS QDs are even more challenging, since the synthesis of ternary nanocrystals (NCs) with well-controlled size, shape, and composition requires a strict balance between the reactivities of three different precursors, to prevent the formation of binary byproducts (*e.g.*, Cu_2S and In_2S_3, rather than CIS) or hetero-NCs (*e.g.*, Cu_2S−CIS).[40] Moreover, CIS QDs produced by direct synthesis are typically trigonal-pyramidal in shape,[52−55] further complicating the determination of their sizes and introducing ambiguities, since "diameter" becomes an ill-defined quantity, leading different authors to use different metrics for the QD size (*e.g.*, average edge length,[55] average diagonal length,[52] Scherrer's diameter determined from powder X-ray diffraction[51,56]).

In this work, we circumvent these difficulties by using topotactic partial Cu^+ for In^{3+} cation exchange to convert template $Cu_{2-x}S$ NCs into nearly spherical and stoichiometric (In/Cu = 0.91 ± 0.11) wurtzite (wz) CIS QDs ranging from 2.7 to 6.8 nm in diameter (size dispersion ≤10%), which are ideally suited to investigate the size-dependence of the band gap and of the molar absorption coefficients at both the first exciton transition energy and far above the band gap (3.1 eV). We also address the size-dependence of the band gap of chalcopyrite (cp) CIS QDs by reanalyzing experimental data published by several groups.[51,52,54−57] Our results demonstrate that the molar absorption coefficients of wz CIS QDs follow a power law with an exponent of 2.45 at first exciton transition energy and scale with the QD volume at 3.1 eV.

RESULTS AND DISCUSSION

Size-Controlled CIS QDs *via* Partial Cation Exchange. Nearly spherical colloidal CIS QDs with small size dispersion (≤10%) were synthesized by partial, self-limited Cu^+ for In^{3+} cation exchange (CE) in template high-chalcocite $Cu_{2-x}S$ NCs, following previously reported procedures (Figure 1a).[58] The

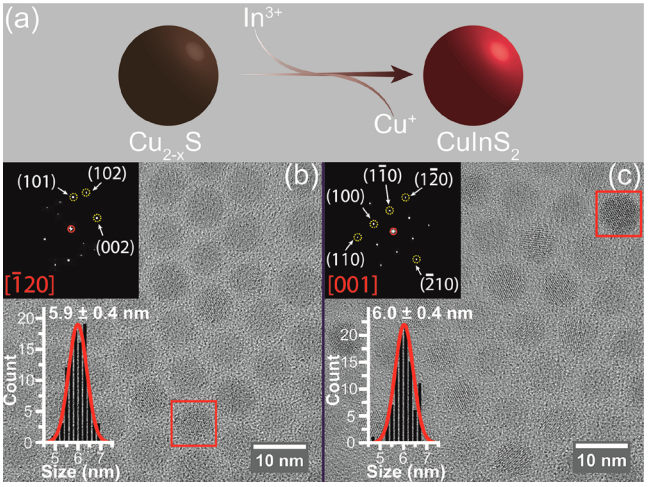

Figure 1. (a) Schematic diagram of partial Cu^+ for In^{3+} cation exchange in template $Cu_{2-x}S$ NCs. (b) High-resolution transmission electron microscopy (HRTEM) image and corresponding size histogram of 5.9 nm template $Cu_{2-x}S$ NCs (polydispersity of 6.8%). The inset shows the Fourier transform (FT) analysis of a single $Cu_{2-x}S$ NC indicated by a red rectangle, which can be indexed to [−120] axial projection of the high chalcocite Cu_2S. (c) HRTEM image and corresponding size histogram of CIS QDs obtained by cation exchange using the $Cu_{2-x}S$ NCs shown in (b) as templates (see Methods for details). The size of the product CIS QDs is 6 nm with a polydispersity of 6.7%. The inset shows the FT analysis of a single CIS QD indicated by a red rectangle, which can be indexed to [001] axial projection of the wurtzite CIS. The size histograms are constructed by measuring over 200 NCs and are fitted to a Gaussian distribution function.

product CIS QDs inherit the shape, size, and polydispersity of the template $Cu_{2-x}S$ NCs (Figure 1b,c). High-resolution transmission electron microscopy (HRTEM) (Figure 1c) and X-ray diffraction (XRD) [Supporting Information (SI), Figure S1] show that the product CIS QDs have the wurtzite crystal structure, demonstrating that the hexagonal sulfide sublattice of the template $Cu_{2-x}S$ NCs is preserved in the product NCs, in agreement with previous reports.[58,59] This protocol is highly versatile and can be applied to obtain CIS QDs in the 2.7−6.8 nm diameter range by using suitable template $Cu_{2-x}S$ NCs (SI, Table S1, Figure S2). The product CIS QDs have a nearly spherical shape and exhibit good TEM contrast, allowing the unambiguous determination of the QD diameters with good accuracy (SI, Figure S2).

Composition and Concentration of the CIS QDs. The composition of the product CIS QDs was determined by inductively coupled plasma optical emission spectroscopy (ICP-OES) analysis and found to be nearly stoichiometric (In/Cu = 0.91 ± 0.11) in the 2.7−6.8 nm size range (Figure 2a). For simplicity, these nearly stoichiometric $Cu_{1.1}In_{0.9}S_2$ QDs will be hereafter referred to as "CIS", without explicit reference to their exact composition, unless the composition is relevant to the point under discussion. To simplify the calculation of the QD concentration, we approximate the In/Cu molar ratio to 1 (see crystallographic model of a single wz CIS QD in Figure 2b). Given that Cu^+ is taken as the reference, the CIS QD concentration can be expressed as follows (see SI, method 1 for details):

$$n_{QDs} = \frac{n_{Cu^+}}{\frac{V_{QD}}{V_{uc}} \times N_{Cu^+/uc}} \quad (1)$$

DOI: 10.1021/acsnano.8b03641
ACS Nano 2018, 12, 8350−8361

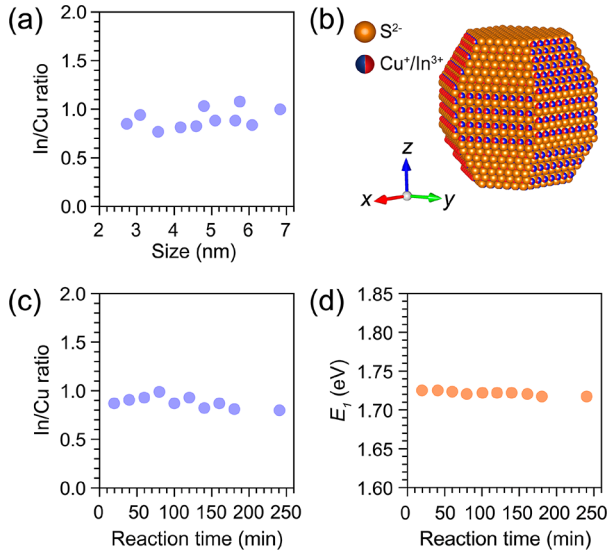

Figure 2. (a) In/Cu molar ratios of wz CIS QDs in a size range from 2.7 to 6.8 nm. (b) Perspective view of the single CIS QD model (Cu^+ or In^{3+} has the same occupation probability). (c) In/Cu molar ratios of wz CIS QDs obtained from 5.5 nm template $Cu_{2-x}S$ NCs. Ten parallel batches of cation exchange reactions were performed by using different reaction times (20−200 min) and In/Cu feeding ratios (1−5), while keeping all other parameters constant (see SI, Table S2 for details). (d) The first excitonic transition energies of the wz CIS QDs extracted from absorption spectra of the samples mentioned in (c).

n_{Cu^+} denotes the molar concentration of Cu^+ measured by ICP-OES analysis. V_{QD} is the volume of a single CIS QD, while V_{uc} represents the volume of the wz CIS unit cell (V_{uc} = 84.99 Å^3),[60] and $N_{Cu^+/uc}$ is the number of Cu^+ ions per unit cell ($N_{Cu^+/uc}$ = 1).[60]

To test the reproducibility and robustness of the synthesis protocol used in our work, 10 different CE reactions were performed using the same batch of 5.5 nm $Cu_{2-x}S$ NCs as templates. The In/Cu feeding ratio was varied from 1 to 5, and the reaction time increased from 20 to 200 min, while keeping all other parameters constant (see SI, Table S2 for details). Interestingly, the In/Cu ratios of the product CIS QDs fluctuated only slightly (average 0.90 ± 0.09) (Figure 2c), regardless of the In/Cu feeding ratio and reaction times. This shows that the Cu^+ for In^{3+} CE in $Cu_{2-x}S$ NCs is self-limited under mild reaction conditions (≤130 °C), in agreement with the model proposed in ref 59, which attributes the self-limitation to the high activation energies required to reorganize the anionic sublattice from hexagonal close-packed in high-chalcocite $Cu_{2-x}S$ and wz CIS to face-centered cubic in In_2S_3.[59] The partial and self-limited character of the Cu^+ for In^{3+} CE in $Cu_{2-x}S$ NCs thus makes the synthesis method developed in our work quite robust and reproducible.

The peak position of the lowest energy absorption transition (E_1) of these 10 CIS QD samples was extracted from the second derivative of their absorption spectra (Figure 2d and SI, Figure S3a) and found to be essentially the same (1.722 ± 0.003 eV), despite the slight composition fluctuations (In/Cu = 0.90 ± 0.09). In contrast, the PL peak positions randomly fluctuate from batch to batch (SI, Figures S3b and S4), probably due to the low photoluminescence quantum yields (PLQYs ≈ 1%) of the samples (SI, Figure S5). This observation implies that the PL peak positions are unreliable quantities to investigate the size dependence of the band gap of CIS QDs. It should be noted that the PL spectra of CIS QD samples with low PLQYs may not necessarily reflect the size, shape, and composition polydispersity of the ensemble, as will be discussed in detail below. The low PL QYs of the wz CIS QD samples investigated here are due to the extensive washing required to ensure that the product QDs were free of unreacted precursors, which resulted in a decrease of the PLQYs of the as-prepared QDs by 1 order of magnitude, likely due to defects induced by the excessive removal of surface ligands.

Size-Dependence of the Optical Transitions of CIS QDs. The absorption and PL spectra of the nearly stoichiometric wz CIS QDs prepared in this work shift to lower energies with increasing NC sizes (Figure 3 and SI,

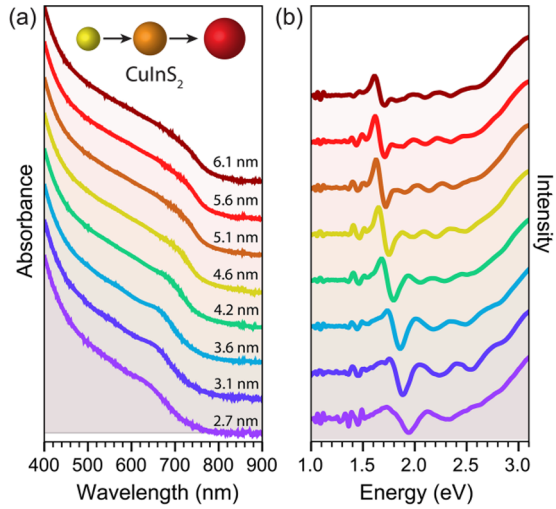

Figure 3. Absorption spectra (a) and corresponding second derivative spectra (b) of wz CIS QDs ranging from 2.7 to 6.1 nm in size.

Figure S6), in agreement with previous reports on both cp and wz CIS QDs.[40,41,51,52,55−58,61] However, it is as yet unclear whether the wide tunability of the optical properties of CIS NCs (and other ternary copper chalcogenides) can be attributed solely to quantum confinement effects, in striking contrast with the II−VI, IV−VI, and III−V binary analogues.[40] The foremost difference between ternary copper (and silver) chalcogenides ($I-III-VI_2$) and binary II−VI and IV−VI compounds is that the former can easily tolerate large deviations from stoichiometry, both in the I/III ratio and VI/(I + III) ratio, resulting in a rich defect chemistry.[62−65] This has a dramatic impact on the optical properties of ternary copper chalcogenides, because the upper valence band in these materials is composed primarily of Cu 3d orbitals hybridized with the p orbitals of the chalcogen, while the conduction band consists of Cu 4s orbitals with some mixing of p character from the group VI element, which makes their band gap composition-dependent.[66] For example, band-gap reductions of up to 190 meV have been reported for bulk CIS upon decreasing the In/Cu ratio from 1.1 to 0.5, accompanied by the development of a low-energy tail extending up to 200 meV below the band gap.[62,63] The potential complications arising from a composition-dependent band gap become particularly relevant at the nanoscale, since CIS NCs are even more tolerant to off-stoichiometry than their bulk counterpart, being

DOI: 10.1021/acsnano.8b03641
ACS Nano 2018, 12, 8350−8361

readily made with In/Cu ratios ranging from 0.34 to 3.33,[67] and also changing composition during the growth process (*e.g.*, In/Cu ratio from 0.58 to 1.09 in the 3.6 to 7.6 nm size range[55]). From this perspective, the small composition and size distributions of the nearly stoichiometric CIS QDs prepared in the present work (*viz.*, In/Cu = 0.91 ± 0.11 and ≤10%, respectively) make them ideally suited to investigate the size-dependence of the optical properties of CIS QDs, without the confounding contribution of significant composition fluctuations. It should also be noted that the size-dependent trends observed in our work are likely also representative of fully stoichiometric wz $CuInS_2$ NCs, given that the deviation from stoichiometry of the investigated CIS QDs is small. The nearly stoichiometric character of the wz CIS QDs studied in the present work is also evidenced by the absence of localized surface plasmon resonance bands, which are typically associated with Cu-rich CIS NCs.[40]

However, as shown above, PL peak positions are less reliable metrics for the size dependence of the band gap of CIS QDs, since they vary significantly even under roughly constant QD size and composition (SI, Figure S4). Moreover, the PL quantum yields of bare CIS QDs are generally low (≤10%),[40,41,54,57,58,61] and therefore the observed PL spectra may not necessarily reflect the size, shape, and composition polydispersity of the ensemble. The inadequacy of the PL peak positions for quantitative studies of the size-dependence of the band gap is further aggravated by the fact that the PL in CIS NCs (and other ternary Cu chalcogenides) is characterized by broad bandwidths [full width at half-maximum (fwhm), ∼200−400 meV] and large global Stokes shifts (Δ_{ST} ≈ 300−500 meV).[40,41,68] For these reasons, the size-dependence of the band gap of CIS QDs will be investigated here using only the peak position of the lowest energy absorption transition, which is more accurate because the absorption spectra are determined by the whole QD ensemble. This is however challenging, as the absorption spectra of CIS NCs are essentially featureless and do not show a sharp first absorption transition, even for QD ensembles with small size dispersion (≤10%), such as those prepared in the present work (Figure 3, SI, Figures S2 and S6). Nevertheless, the first absorption transition energy (E_1) can be reliably determined by locating the minimum of the second derivative of the absorption spectrum (Figure 3). It should be noted that the absorption spectra of colloidal QDs might be distorted by the presence of absorbing impurities. Therefore, the evaluation of the CIS QD purity prior to acquisition of the absorption spectra is essential (see Methods for details). As observed in Figure 3, the E_1 values are clearly size-dependent. This size-dependence will be quantitatively addressed below, after we have discussed the spectral characteristics of CIS QDs in more detail.

As mentioned above, the optical spectra of CIS NCs are characterized by broad features, in both absorption and PL.[40,41,52,54,58,68] However, only the PL fwhm's have been quantitatively discussed in the literature, probably because they can be readily obtained from the PL spectra. In contrast, the fwhm of the lowest energy absorption transition can only be extracted from the absorption spectra by fitting a Gaussian distribution function centered at the peak position determined from the second derivative of the spectra (SI, Figure S7). We performed this analysis for the wz CIS QDs prepared in our work and found that the fwhm of the lowest energy absorption transition varies from 180 to 320 meV, while that of the PL peak ranges from ∼300 to 420 meV (SI, Figure S8). For comparison, we also analyzed wz CIS QDs that had been investigated in our previous work.[58] These samples have similar compositions to those investigated in the present work (*viz.*, In/Cu = 0.7 ± 0.1), but present higher PLQYs (22% to 3.4% in the 5.4 to 7.2 nm size range)[58] and therefore yield more reliable PL fwhm values. It can be seen that the fwhm values of these samples are comparable to those of the wz CIS QDs prepared in the present work, except for the PL fwhm of the QD samples with $d \geq 5$ nm, which are significantly larger for the presently investigated samples (*viz.*, 420−380 and 320−300 meV, respectively, SI, Figure S8). This difference can be attributed to the lower PLQYs of the samples investigated in the present work, which result in PL spectra with higher signal-to-noise ratios and therefore less reliable PL fwhm. Taken together, the data obtained from both groups of samples suggest that the PL fwhm is essentially size-independent (∼300−320 meV in the 2.7 to 7.2 nm diameter range, neglecting the values obtained for the QDs prepared in the present work with $d \geq 5$ nm), while that of the lowest energy absorption peak decreases with size from ∼300 to ∼200 meV in the 2.7 to 7.2 nm diameter range. We have also determined the global Stokes shifts (Δ_{ST}) of the wz CIS QDs investigated in the present work and in our previous work[58] and established that they are size-independent (*viz.*, 455 ± 27 meV in the 2.7 to 7.2 nm size range, SI, Figure S8). This is in contrast with the weakly size-dependent Δ_{ST} values (*viz.*, 470 to 350 meV in the 2.5 to 5.1 nm size range) previously reported for cp CIS QDs.[52] The discrepancy is unlikely to be due to the different crystal structures (wz and cp), since very similar Δ_{ST} values have been reported for similarly sized cp CIS QDs (*viz.*, 460 meV for 2.2 nm NCs,[57] 436 meV for 2.5 nm NCs[54]). The fwhm's observed here for the PL peaks are also comparable to those previously reported for cp CIS NCs.[40,41,52,54,68]

The characteristics of the PL of CIS NCs (*viz.*, broad fwhm: 200−400 meV, large Δ_{ST}: ∼300−500 meV, and long radiative lifetimes τ: ∼200−400 ns)[40,41,68] are strikingly different from those of the $1S_h-1S_e$ band-edge PL of the prototypical II−VI NCs (*e.g.*, fwhm: 150 to 80 meV,[69,70] Δ_{ST}: ∼21 ± 4 meV,[69] and τ: 18−40 ns,[25] for ensembles of CdSe QDs in the 2.6 to 8 nm size range with ≤10% size dispersion), indicating that the radiative recombination mechanisms in these two classes of materials are fundamentally dissimilar in nature. The origin of the PL of CIS (and other ternary Cu and Ag chalcogenides) NCs has been under intense debate[40] and likely involves the radiative recombination of a delocalized conduction band electron with a localized hole.[54,58,71−73] The hole localization after photoexcitation occurs on subpicosecond time scales, probably on a Cu^+ ion.[54,73] We note that the larger variability of the PL peak positions of CIS NCs with respect to the absorption transitions (see discussion above and SI, Figure S4) is consistent with this radiative recombination model and can be accounted for by the inherently stochastic nature of the hole localization process.

However, the radiative recombination model presented above cannot account for the broad bandwidths observed for the lowest energy absorption transition of CIS QDs (∼200−300 meV, which is twice as large as those observed for CdSe QDs[69,70] and ∼4 times larger than those reported for PbSe QDs[74]), since the line widths of absorption transitions in semiconductor QDs cannot be affected by the localization of the photogenerated hole. A possible explanation can be found in a recent theoretical paper by Efros and co-workers,[75] which proposes that the PL of spherical cp CIS NCs originates from

DOI: 10.1021/acsnano.8b03641
ACS Nano 2018, 12, 8350−8361

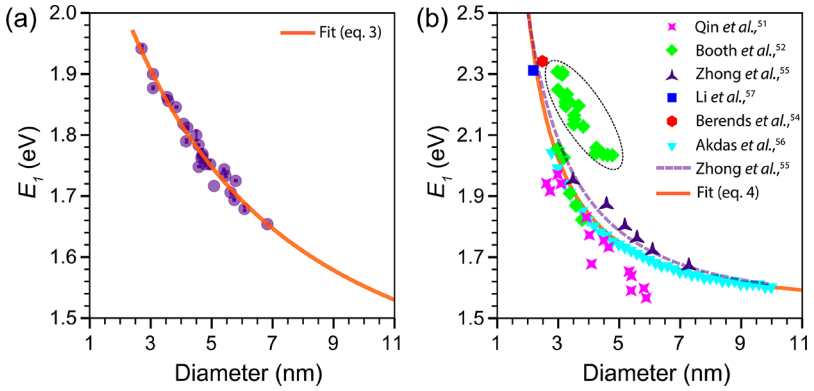

Figure 4. (a) Sizing curve of colloidal wz CIS QDs (In/Cu = 0.91 ± 0.11). The solid line is a fit based on a theoretical expression (eq 2) and is described by eq 3. (b) Sizing curve of colloidal cp CIS QDs. The symbols represent experimental data collected from previous reports.[51,52,54−57] The In/Cu ratio of most samples is 1.0 ± 0.1 (see Supporting Information, Table S3, for the reported composition of all samples). The composition of the CIS QDs studied by Zhong *et al.*[55] and Li *et al.*[57] were reported to be size-dependent (In/Cu = 0.42 to 0.88 in the 3.6 to 7.6 nm size range[55] and 1.04 to 0.93 in the 2.2 to 3.3 nm size range,[57] respectively). The purple dashed line represents a calculation based on a finite depth-well effective mass approximation model.[55] The orange solid line is a fit based on a theoretical expression (eq 2) and is described by eq 4. The green data points circled by the dashed ellipsoidal line are derived from an empirical polynomial function reported by Booth *et al.* using their data[52] and was not included in the fit (see text for further details). For convenience, sizing curves correlating the QD diameter with the wavelength of the first absorption peak are provided in the Supporting Information (Figure S9).

the $1S_h-1S_e$ exciton transition, similarly to the cases of the binary II−VI, IV−VI, and III−V QDs. The exciton radiative recombination in this model thus precludes the involvement of localized carriers. The characteristics of the PL of CIS QDs are attributed to the nature of the $1S_h-1S_e$ exciton fine-structure states, of which the lowest emitting state is nominally a dark exciton that hardly contributes to the absorption and is separated by a large size-dependent energy gap from three upper bright fine-structure states, which account for most of the absorption oscillator strength.[75] This model thus explains both the large Δ_{ST} values and long radiative lifetimes associated with the PL of CIS QDs and can also explain the broad (and size-dependent) line widths of the lowest energy absorption transition, as the energy separation between the highest and the lowest energy bright states varies from 100 to 30 meV in the 2 to 3.6 nm diameter range.[75] Nevertheless, this model also predicts a strongly size-dependent Stokes shift (*viz.*, 300 to 100 meV in the 2 to 3.6 nm diameter range), in contrast to the size-independent Stokes shift (*viz.*, 455 ± 27 meV in the 2.7 to 7.2 nm size range) observed in the present work. This model is also unable to explain the broad and (essentially) size-independent PL fwhm displayed by CIS QDs, which suggests that the emitting state is subject to a strong exciton−phonon coupling. We note that a strong exciton−phonon coupling could also explain the broad bandwidths of the lowest energy absorption transition of CIS QDs, but this explanation lacks as yet experimental and theoretical support. It is thus clear that the full understanding of the exciton transitions in both cp and wz CIS QDs requires further experimental and theoretical work.

Sizing Curves for wz and cp CIS QDs. To shed light on the size-dependence of the band gap of CIS QDs, we constructed empirical sizing curves for both wz and cp CIS QDs (Figure 4). The peak positions of the lowest energy absorption transition (E_1) of wz CIS QDs were extracted from the second derivative of the absorption spectra of the nearly stoichiometric (In/Cu = 0.91 ± 0.11) CIS QDs prepared in our work (Figure 3), while the QD diameters were determined from TEM images (SI, Figure S2). The data points for cp CIS QDs were collected from previous reports[51,52,54−57] and were mostly obtained from nearly stoichiometric QDs, with In/Cu ratios of 1.0 ± 0.1 (see Supporting Information, Table S3, for the reported composition of all the cp CIS QDs included in Figure 4b). The composition of the cp CIS QDs studied by Zhong *et al.* were reported to be size-dependent, changing from In/Cu = 0.42 to 0.88 in the 3.6 to 7.6 nm size range.[55] A modest size-dependence of the composition was also observed by Li *et al.* (In/Cu = 1.04 to 0.93 in the 2.2 to 3.3 nm size range).[57] It should be noted that the sizes and E_1 values for cp CIS QDs were not all determined in the same way. For instance, the effective QD diameter was taken to be the edge length of the pyramidal NCs by Zhong *et al.*,[55] while Booth *et al.*[52] took their height (*i.e.*, the diagonal length of the 2D TEM projections), and Qin *et al.*[51] and Akdas *et al.*[56] used the Scherrer's diameter determined from powder X-ray diffraction. The E_1 values were also determined by using different methods (*e.g.*, extrapolation of Tauc plots in ref 55, double-tangent method in ref 51). Nevertheless, as we will show below the uncertainties and systematic errors associated with individual reports, as well as the compositional variations between CIS QD samples investigated in different studies, are averaged out when the combined data set is analyzed as a whole.

To fit the empirical size-dependent trends shown in Figure 4, we used an expression previously proposed by Allan and Delerue based on tight binding calculations:[76]

$$E_g(d) = E_g(\infty) + \frac{1}{ad^2 + bd + c} \quad (2)$$

where $E_g(d)$ and $E_g(\infty)$ are the band gap (in eV) for a QD of diameter d (in nm) and for bulk, respectively, and a, b, and c are constants. Equation 2 has been successfully used to fit the empirical trends observed for PbSe,[28,76] PbS,[23] CdSe,[25] and CdTe[25] QDs. Fitting the experimental data for wz CIS QDs (Figure 4a) to eq 2 yields ($\chi^2 \approx 0.9999$):

$$E_g(\text{wz\_CIS}) = 1.327 + \frac{1}{0.0125d^2 + 0.225d + 0.938} \quad (3)$$

Interestingly, the $E_g(\infty)$ value obtained from the fit (1.327) is very close to the bulk band gap of wz CIS calculated by

DOI: 10.1021/acsnano.8b03641
ACS Nano 2018, 12, 8350−8361

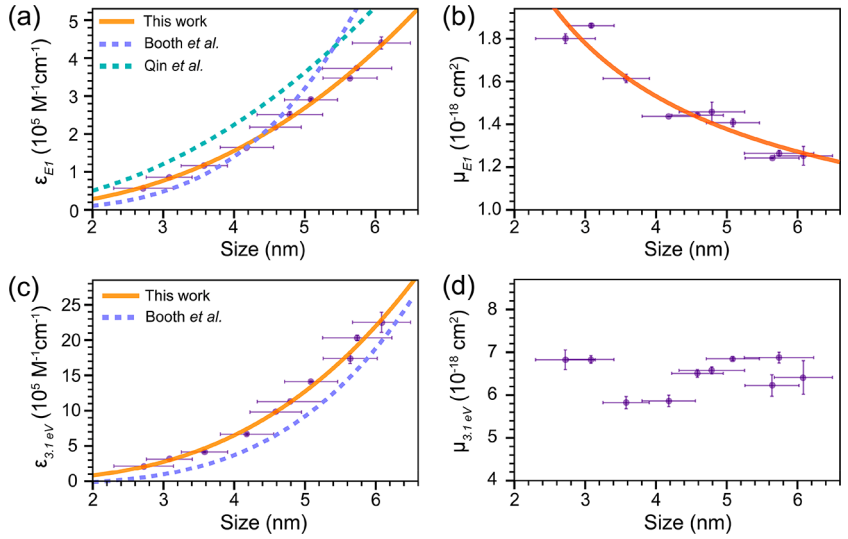

Figure 5. (a) Size-dependent molar absorption coefficients ε_{E_1} at the first exciton transition energy (E_1) of nearly spherical wz CIS QDs (In/Cu = 0.91 ± 0.11). The orange solid line is a fit to the data using a power law function (eq 6). Purple and green dashed lines denote the size-dependent trends reported in the literature for pyramidal cp CIS QDs (In/Cu = 0.91 and ~1).[51,52] (b) Size-dependent absorption cross-section per formula unit at E_1(μ_{E_1}) of wz CIS QDs (In/Cu = 0.91 ± 0.11). The orange solid line is a fit to the data using a power law function (eq 9). (c) Size-dependent molar absorption coefficients $\varepsilon_{3.1\ eV}$ at 3.1 eV of wz CIS QDs (In/Cu = 0.91 ± 0.11). The orange solid line is a fit to the data using a power law function (eq 11). The purple dashed line denotes the size-dependent trend reported in the literature for pyramidal cp CIS QDs (In/Cu = 0.91) by Booth *et al.*[52] (d) Size-dependent absorption cross-section per formula unit at 3.1 eV ($\mu_{3.1\ eV}$) of wz CIS QDs (In/Cu = 0.91 ± 0.11).

Tomić and co-workers using hybrid density functional theory (DFT) (*viz.*, 1.3 eV).[77] Bulk wz CIS is metastable at room temperature, and therefore experimental data on its band gap have only recently become available, owing to the development of synthesis methods yielding ensembles of large wz CIS nanoparticles.[60,78] The reported band-gap values, however, still carry a significant uncertainty and are spread over a wide range (*viz.*, 1.10−1.23 eV in ref 60 and 1.42 eV for 20 nm NCs in ref 78). Nevertheless, it is clear that the band gap of wz CIS is smaller than that of cp CIS, which explains why wz CIS QDs typically show PL at lower energies than similarly sized cp CIS QDs.[58,68] This is also consistent with the expression obtained by fitting the experimental data for cp CIS QDs (Figure 4b) to eq 2 ($\chi^2 \approx 0.9997$):

$$E_g(\text{cp\_CIS}) = 1.532 + \frac{1}{0.0882d^2 + 0.587d - 0.517} \quad (4)$$

which yields a $E_g(\infty)$ value that agrees very well with the band gap reported for bulk cp CIS (*viz.*, 1.535 eV at 300 K).[79] We note that some data points (indicated by the dashed ellipsoid in Figure 4b) were not included in the fit because they clearly deviated from the general trend evidenced by the other data points. The excluded data points were obtained from an empirical sizing curve reported by Booth and co-workers,[52] which was constructed using PL peak positions. To make these E_1 values comparable to the values extracted from absorption data, we corrected them by using the size-dependent Stokes shifts reported in the same work.[52] The evident discrepancy between this group of data points and the E_1 values extracted directly from absorption spectra (including the spectra reported by Booth and co-workers in ref 52) clearly demonstrates the inadequacy of PL peak positions as metrics for the band gap, as discussed in detail above. A systematic error can also be identified in the data reported by Qin *et al.*[51] for cp CIS QDs with diameters equal to or larger than 4 nm, probably due to the large uncertainties associated with the determination of E_1 by the double-tangent method in absorption spectra with broad and indistinct peaks.

The fitting results (eqs 3 and 4) show that the increase in band gap with the reduction of the CIS QD size is mainly determined by the $1/d$ term, for both wz and cp QDs. The contribution of the $1/d^2$ term only becomes relevant for sufficiently small QDs. This is in striking contrast with the size-dependence of the band gap reported for CdSe and CdTe QDs, which is almost completely due to the $1/d^2$ term,[25] but is analogous to that observed for PbSe and PbS QDs, which also varies mainly with $1/d$.[23,28,76] The $1/d^2$ term is typically associated with the quantum confinement contribution, since this is the dependence predicted based on the effective mass approximation (EMA), while the $1/d$ dependence reflects the Coulomb interaction contribution.[80] However, the contribution of the Coulomb interaction decreases with increasing dielectric constant ε[80] and should thus not be significant for CIS QDs (ε = 10).[81] Therefore, the dominance of the $1/d$ term can be interpreted as evidence that, similarly to the Pb-chalcogenides, the energy dispersion is mostly linear around the band gap, being parabolic only in a very small region near the extrema (*i.e.*, top of valence band and bottom of conduction band).[76] This implies that the hole and electron effective masses should not be relevant quantities to determine the extent of quantum confinement effects in CIS QDs. However, it is clear that the size-dependence of the band gap of cp CIS QDs is much stronger than that of wz CIS QDs (see Figure 4a and b and eqs 3 and 4). A possible explanation for this difference can be found in the electron and hole effective masses of the two materials, which are smaller for cp CIS (*viz.*, m_e = 0.153 m_0, m_h = 0.958 m_0)[77] than for wz CIS (*viz.*, m_e = 0.173 m_0, m_h = 2.181 m_0).[77] Since the experimental effective masses for wz CIS are not yet known, we compared theoretical values calculated by hybrid DFT for both wz and cp CIS.[77]

DOI: 10.1021/acsnano.8b03641
ACS Nano 2018, 12, 8350−8361

However, it should be pointed out that the calculated values for cp CIS are slightly different from the experimental ones (*viz.*, m_e = 0.16 m_0, m_h = 1.3 m_0).[55]

We note that a model based on the EMA (*viz.*, the finite depth-well EMA)[82] has been successfully used by Zhong and co-workers[55] to describe the empirical size-dependence observed in their work for cp CIS QDs (3.6 to 7.3 nm; see dashed line in Figure 4b, parameters used: m_e= 0.16 m_0, m_h = 1.3 m_0; $E_{g(bulk)}$ = 1.53 eV; $E_{g(cap)}$ = 7 eV). This modified EMA model takes into account the fact that the confinement potential V_0 is finite and estimates it as being the difference between the HOMO−LUMO energy gap of the capping ligands and the band gap of the semiconductor ($V_0 = [E_{g(cap)} - E_{g(bulk)}]/2$).[82] However, Figure 4 clearly shows that the fit based on eq 2 (*i.e.*, eq 4 above) is more accurate over the whole QD size range analyzed than the calculations based on the modified EMA (dashed line). The sizing curves reported in the present work (Figure 4 and eqs 3 and 4) thus offer a convenient and accurate way of determining the sizes of both wz and cp CIS QDs directly from absorption spectroscopy measurements. For convenience, sizing curves directly correlating the QD diameter with the wavelength of the first absorption peak are provided in the Supporting Information (Figure S9).

Molar Absorption Coefficient of wz CIS QDs at the First Exciton Transition Energy. The molar absorption coefficients ε of CIS QDs can be obtained using the Beer−Lambert law:

$$A = \varepsilon c l \tag{5}$$

where A is the measured absorbance at the lowest energy absorption transition E_1 (*i.e.*, the first exciton transition $1S_h$−$1S_e$), c denotes the molar concentration of CIS QDs, and l is the optical path length. The concentration of CIS QDs is obtained as discussed above (see also SI, method 1, for details). The peak positions E_1 were extracted from the second derivative of the absorption spectra as described above. The size-dependent molar absorption coefficients at the first exciton transition energy (ε_{E1} in 10^5 $M^{-1}\cdot cm^{-1}$) of CIS QDs can thus be readily obtained (Figure 5a). We observed that CIS QDs larger than 6.1 nm tend to lose their colloidal stability after extensive purification, which results in the formation of aggregates that introduce light-scattering contributions to the measured absorption spectra. This issue affects the accuracy of the determination of absorption coefficients; thus data concerning CIS QDs larger than 6.1 nm are not included in Figure 5.

Similarly to previous work on binary InAs,[37,38] Cd-chalcogenide,[25,29,31−33] and Pb- chalcogenide QDs,[23,26,28,30] the data in Figure 5a can be fitted to a power law as follows (χ^2 = 0.999):

$$\varepsilon_{E_1} = 5208 d^{2.45} \tag{6}$$

It is evident that the size-dependence observed in our work is significantly different from those reported by both Qin and co-workers (*viz.*, $11430d^{2.147}$)[51] and Booth and co-workers (*viz.*, $(830 \pm 660)d^{3.7\pm0.6}$).[52] Moreover, the absolute ε_{E_1} values in both reports are overestimated with respect to those presented here (in the case of Booth *et al.* only for d <4.5 nm). As discussed above, these discrepancies likely originate from the inherent experimental difficulties associated with the accurate determination of the effective diameter of trigonal-pyramidal NCs (which may or may not be truncated depending on the size), peak positions from broad and indistinct absorption spectra, and concentrations of ternary QDs that may have significant compositional polydispersity. The combined effect of these uncertainties may be very large, especially considering that the QD concentrations are affected by the uncertainties in both their size and composition. Moreover, colloidal stability issues may introduce additional errors due to light-scattering contributions, which may go unnoticed given the typically featureless aspect of the absorption spectra of CIS NCs.

The molar absorption coefficient ε is related to the absorption cross-section per QD σ by[25,30,33,38]

$$\varepsilon = \frac{\sigma N_A}{2303} \tag{7}$$

where N_A is Avogadro's constant. The absorption cross-section per formula unit μ is given by[25]

$$\mu = \frac{\sigma}{N_{unit/QD}} = \frac{\sigma V_{uc}}{Z V_{QD}} = \frac{V_{uc}}{Z V_{QD}} \frac{2303\varepsilon}{N_A} \tag{8}$$

where $N_{unit/QD}$ denotes the number of unit cells per QD. The number of formula units per unit cell (Z = 1) can be obtained from the crystal lattice parameters of wz CIS QDs.[60] As shown in Figure 5b, the absorption cross-section per formula unit at the first exciton transition energy (μ_{E_1}) of wz CIS QDs is size-dependent and can be described as (χ^2 = 0.998):

$$\mu_{E1} = 6.298 \times 10^{-19} + 2.940 \times 10^{-18} d^{-0.882} \tag{9}$$

This size-dependence strongly deviates from the theoretically expected one, since a nearly size-independent oscillator strength per QD is predicted for the first exciton transition $1S_h$−$1S_e$ by several theoretical models (*viz.*, k·p EMA,[80,83] tight-binding,[84] and effective bond-orbital model[85]), which implies that μ_{E_1} should follow a $1/d^3$ dependence. Nevertheless, discrepancies between this theoretical prediction and empirical trends are commonly observed. For example, a $1/d^2$ dependence has been reported for a number of colloidal QD systems (CdSe QDs with d = 1.5−8 nm,[25,33] CdTe QDs with d = 3.5−9 nm,[25] PbSe QDs with d = 3−8 nm,[28] and CdS QDs with d = 2.4−5.6 nm[35]). To date, a $1/d^3$ dependence has only been reported for CdTe QDs with d = 2−4 nm[25,86] and CdS QDs with d = 1.3−2.4 nm.[35] The reasons for the divergence between the theoretical prediction and the experimental observations remain as yet unclear. Furthermore, it is important to note that the strong size-dependence of the absorption coefficient of the lowest energy absorption transition of colloidal QDs makes it less suitable as a tool to determine QD concentrations, since its accuracy may be strongly compromised by the size and shape polydispersity of the sample under consideration.

Molar Absorption Coefficient of CIS QDs at Energies Far above the Band-Edge. The molar absorption coefficient at higher energy (3.1 eV) of the wz CIS QDs prepared in this work can be obtained by

$$\varepsilon_{3.1eV} = \frac{A_{3.1eV}}{A_{E_1}} \varepsilon_{E_1} \tag{10}$$

where $A_{3.1\ eV}$ and A_{E_1} are the absorbances at 3.1 eV and at the first exciton transition energy, respectively. The obtained data

DOI: 10.1021/acsnano.8b03641
ACS Nano 2018, 12, 8350−8361

were plotted with respect to the CIS QD diameter (d) (Figure 5c) and fitted to a power function yielding (χ^2 = 0.998)

$$\varepsilon_{3.1\text{eV}} = 10175d^3 \quad (11)$$

It is interesting to note that the $\varepsilon_{3.1\text{ eV}}$ values scale with the volume of QDs, showing that the spectral density of states is no longer significantly affected by quantum confinement effects. This has been experimentally observed for a number of colloidal QD systems (CdSe,[24,25,33,87] CdTe,[25] PbSe,[28] InAs[38]) and is consistent with theoretical predictions based on the EMA model.[87] In contrast, the size-dependence of $\varepsilon_{3.1\text{ eV}}$ reported by Booth and co-workers for cp CIS QDs (*viz.*, $(2123 \pm 1090)d^{3.8\pm0.3}$)[52] is far stronger than the theoretical expectation and the previous experimental observations. The reasons for the inconsistency between the present results and those previously reported in ref 52 are probably the same as already discussed above for the size-dependence of the ε_{E_1} values. The absorption cross-section per formula unit at 3.1 eV ($\mu_{3.1\text{ eV}}$) can be determined by applying eq 8 above and is observed to be size-independent over the whole size range investigated in our work (Figure 5d). These results confirm that $\varepsilon_{3.1\text{ eV}}$ scales with the volume of the CIS QDs and imply that $\varepsilon_{3.1\text{ eV}}$ is a more reliable parameter to accurately determine the concentrations of colloidal suspensions of CIS QDs.

The fact that the absorption cross-sections per unit cell at sufficiently high energies above the band gap are size-independent implies that they can be estimated from bulk optical constants. This is indeed the case, as has been demonstrated for a number of materials (*e.g.*, CdSe,[25,87] InAs[38]). The absolute absorption cross-section per formula unit of both wz and cp CIS QDs at 3.1 eV can then be calculated based on the Bruggeman effective media theory,[25,33,88] which can be written as

$$\mu_{\text{th}-3.1\text{ eV}} = \frac{\sigma_{\text{th}}}{N_{\text{unit/QD}}} = \frac{V_{\text{uc}}}{z}\frac{n}{n_s}|f_{\text{LF}}|^2\,\alpha_{3.1\text{ eV}} \quad (12)$$

where n_s and n are respectively the refractive indices of the solvent (1.5 for toluene) and the semiconductor at 3.1 eV (2.636 for wz CIS[89] and 2.795 for cp CIS[79]). $\alpha_{3.1\text{ eV}}$ is the absorption coefficient of bulk CIS QDs at 3.1 eV (1.9×10^5 cm^{-1} for wz CIS and 2.55×10^5 cm^{-1} for cp CIS), which is calculated by[90]

$$\alpha_{3.1\text{ eV}} = \frac{4\pi}{\lambda}k(\lambda) \quad (13)$$

where λ is the wavelength of light in the vacuum. k denotes the extinction coefficient of bulk CIS at 3.1 eV (0.605 for wz CIS[89] and 0.813 for cp CIS[79]).

The term f_{LF} in eq 12 is the local field correction factor, which is given by[25,33,88]

$$f_{\text{LF}} = \frac{3m_2^2}{m_1^2 + 2m_2^2} \quad (14)$$

m_1 ($m_1 = n - ik$) and m_2 are the complex refractive indices of the semiconductor and solvent, respectively. Since the absorption of toluene at 3.1 eV is negligible, m_2 can be replaced by n_s (*viz.*, 1.5). The absolute absorption cross-section per formula unit of wz and cp CIS at 3.1 eV is thus calculated to be 9.7×10^{-18} and 1.18×10^{-17} cm^2, respectively. It should be noted that the bulk optical constants (n and k) used for wz CIS are theoretical values obtained by DFT calculations,[89] since experimental data are available only for bulk cp CIS. Nevertheless, the calculated $\mu_{3.1\text{ eV}}$ value of wz CIS is very close to that of cp CIS QDs, and they are both in good agreement with the value experimentally determined in our work for wz CIS QDs [$\mu_{3.1\text{ eV}} = (6.3 \pm 0.4) \times 10^{-18}$ cm^2]. This demonstrates that the absorption cross-section of CIS QDs at high energies can be indeed deduced from the bulk optical constants.

CONCLUSIONS

We have reported here a detailed study of the size-dependence of the optical properties of colloidal wz CIS QDs in the 2.7 to 6.1 nm diameter range, with emphasis on the energy of the first absorption transition ($1S_e-1S_h$) and its absorption coefficient ε_{E_1} and on the absorption coefficient at higher energy (3.1 eV). Nearly spherical wz CIS QDs with small size dispersion (≤10%) are synthesized by self-limited topotactic partial Cu^+ for In^{3+} cation exchange in template $Cu_{2-x}S$ NCs. This synthesis protocol is robust and highly reproducible, yielding nearly stoichiometric CIS QDs with very small composition variations (In/Cu = 0.91 ± 0.11), regardless of their sizes. The well-defined nearly spherical size and small composition and size distributions of the CIS QDs prepared in the present work make them ideally suited to this study. Our results show that the band gap of wz CIS QDs increases with decreasing QD size, following a trend that depends primarily on $1/d$. A sizing curve is also constructed for cp CIS QDs by collecting and reanalyzing data published by several different groups.[51,52,54−57] The size-dependence of the band gap of cp CIS QDs is observed to be slightly stronger than that of wz CIS QDs, but also follows primarily a $1/d$ dependence. These sizing curves provide a convenient and accurate way of determining the sizes of both wz and cp CIS QDs directly from absorption spectroscopy measurements. Moreover, we find that the experimental size dependence of the molar absorption coefficient ε_{E_1} of wz CIS QDs at the first exciton transition energy can be accurately fit by the expression $\varepsilon_{E_1} = 5208d^{2.45}$. Interestingly, we observe that the absorption coefficients of the wz CIS QDs at energies far above the band gap (*i.e.*, 3.1 eV) scale directly with the QD volume, which implies that the absorption cross-sections per unit cell are size-independent and therefore can be estimated from bulk optical constants. Indeed, the absolute absorption cross-sections per formula unit calculated from the bulk optical constants of wz and cp CIS at 3.1 eV (*viz.*, 9.7×10^{-18} and 1.18×10^{-17} cm^2, respectively) are in good agreement with the value experimentally determined in our work for wz CIS QDs [$(6.3 \pm 0.4) \times 10^{-18}$ cm^2]. These results demonstrate that the absorption coefficients at 3.1 eV are better suited to determine the concentrations of colloidal suspensions of CIS QDs, since they are less sensitive to size and shape dispersion.

METHODS

Materials. Copper(I) acetate (CuAc, 97%), indium acetate ($In(Ac)_3$, 99.99%), 1-dodecanethiol (DDT, ≥98%), trioctylphosphine (TOP, 90%), trioctylphosphine oxide (TOPO, 99%), 1-octadecene (ODE, 90%), nitric acid (HNO_3, 69.5%), anhydrous toluene, methanol, and butanol were purchased from Sigma-Aldrich. Multi-Element calibration standard 3 and Multi-Element calibration standard 5 (10 μg/mL of each element) were purchased from PerkinElmer. TOPO and ODE were degassed at 120 °C under vacuum overnight prior to synthesis. Other reagents were used as received. The chemicals were weighed and handled inside a glovebox.

DOI: 10.1021/acsnano.8b03641
ACS Nano 2018, 12, 8350−8361

Synthesis of $Cu_{2-x}S$ NCs. Template $Cu_{2-x}S$ NCs were synthesized in a standard Schlenk line according to previously reported procedures.[58] CuAc (1 mmol, 0.126 g) and TOPO (4.65 mmol, 1.834 g) were mixed with 10 mL of predegassed ODE in a 100 mL three-neck flask. The mixture was degassed at 100 °C for 1 h. Then, the flask was purged by N_2 and further heated to 210 °C. At 160 °C, 2.5 mL of DDT were swiftly injected accompanied by a sharp decrease of temperature to 147 °C. A change in solution color from dark green to brown indicates the nucleation and growth of $Cu_{2-x}S$ NCs. These NCs were allowed to grow at 210 °C for 5−70 min, followed by naturally cooling to room temperature. The crude reaction products were washed using isometric butanol and methanol, followed by centrifugation at 3000 rpm for 10 min. The washing step was repeated twice to remove residual precursors. Finally, the purified $Cu_{2-x}S$ NCs were dispersed into 5 mL of anhydrous toluene and stored in a glovebox for further use.

Synthesis of CIS QDs. The wz CIS QDs were prepared following previously published procedures.[58] A 1 mL amount of purified $Cu_{2-x}S$ NCs was degassed to remove toluene and was then redispersed into a solution of DDT (0.5 mL) and ODE (1.5 mL). In the meantime, $In(Ac)_3$ (0.2 mmol, 0.0584 g), TOP (0.2 mmol, 100 μL), and 2 mL of ODE were mixed and degassed at 125 °C for 1 h. Subsequently, the reaction flask containing the In−TOP complex (In/TOP = 1) solution was refilled with N_2 and maintained at 125 °C. After that, the aforementioned $Cu_{2-x}S$ NCs solution was swiftly injected into the In−TOP complex solution under N_2. The mixture was kept at 125 °C for a variable amount of time depending on the size of template $Cu_{2-x}S$ NCs (see SI, Table S1 for details). The mixture was vigorously stirred, then naturally cooled to room temperature. The crude reaction mixture was directly centrifuged at 2500 rpm for 1 min to isolate unreacted precursors. The supernatant was collected and the product CIS QDs were isolated and extensively washed (at least three times), using the same purification procedure described above. Occasionally, the solution became a gel after cooling or during the washing, requiring the addition of a few drops of octylamine to redisperse the QDs and proceed with the washing cycles. Finally, the CIS QDs were dispersed into 4 mL of anhydrous toluene, well-sealed, and stored in a glovebox for further use.

Assessment of the Sample Purity. Prior to the ICP-OES analysis and absorption spectroscopy measurement, the purity of the CIS QDs was assessed by XRD after different steps of purification. Since the indium source in the CE reaction is $In(Ac)_3$, which is insoluble in nonpolar solvents, residual $In(Ac)_3$ may still be present after the reaction. To remove $In(Ac)_3$, the crude samples were directly centrifuged without adding any antisolvents, followed by collecting suspended QDs in supernatant. This step essentially removes unreacted $In(Ac)_3$, as evidenced by XRD measurements (SI, Figure S10). The suspended QDs in the supernatant were subsequently washed, using the same purification procedure described above, for at least three times to ensure complete removal of $In(Ac)_3$ and other byproducts. After this purification step, the CIS QDs were dispersed into anhydrous toluene and were stored in a glovebox.

Optical Spectroscopy. Prior to optical measurements, the quartz cuvettes were immersed in 69.5% nitric acid for 5 min, then thoroughly rinsed with Milli-Q water and absolute ethanol for a final rinse, and dried by compressed air flow. This step is crucial for reducing experimental error caused by contaminations from the cuvettes. Samples for optical measurements were prepared by dispersing CIS QDs into 3 mL of anhydrous toluene in precleaned sealable quartz cuvettes under N_2. To reduce inner filter effects, the optical density at the lowest energy transition was below 0.1. Absorption spectra were recorded on a double-beam PerkinElmer Lambda 950 UV/vis/NIR spectrometer (175−3300 nm). PL spectra were acquired using an Edinburgh Instruments FLS920 spectrofluorometer equipped with a 450 W Xe lamp as excitation source and double-grating monochromators for both the excitation and the emission. A Hamamatsu R928 photomultiplier tube (250−800 nm) and a liquid N_2 cooled Hamamatsu R5509-72 photomultiplier tube (750−1600 nm) were used as detectors for obtaining PL spectra.

Photoluminescence Quantum Yields. The PLQYs were measured using indocyanine green (ICG, PLQY = 12%) in DMSO as a standard.[58,91] To avoid inner filter effects, the absorbances of the QD and ICG solutions at and above the excitation wavelength (678 nm) were below 0.1.

X-ray Diffraction. XRD results were recorded on a Bruker D2 Phaser, equipped with a Co Kα X-ray source (1.790 26 Å). Samples were washed at least three times, dried under vacuum overnight, and uniformly dispersed on a silicon wafer prior to XRD measurements.

Transmission Electron Microscopy (TEM). Conventional TEM images were acquired using a FEI Tecnai-20 microscope operating at 200 kV. HRTEM was performed on a FEI Talos F200X microscope operating at 200 kV. The lattice spacings of NCs were obtained by Fourier transform from the area of interest in HRTEM images. Samples for TEM imaging were prepared by drop-casting a toluene solution of purified NCs onto a carbon-coated 200 mesh copper TEM grid.

Inductively Coupled Plasma Optical Emission Spectroscopy. ICP measurements were performed on a PerkinElmer Optima 8300 ICP-OES spectrometer equipped with a high-performance segmented-array charge-coupled-device detector. Samples were carefully dried under vacuum overnight and then thoroughly dissolved in HNO_3 (69.5%), yielding clean yellow solutions. This solution was further diluted by 1000 times to reach the ppm ranges required for the measurement. In the meantime, Cu^+ and In^{3+} calibration curves were prepared using Multi-Element calibration standard 3 (10 μg/mL of each element in 5% HNO_3) with trace concentrations ranging from 0 to 1 ppm. S^{2-} calibration curves were prepared using Multi-Element calibration standard 5 (10 μg/mL of each element in H_2O with a trace of HF) with trace concentrations ranging from 0 to 1 ppm. All the calibration curves were fitted to lines with *R*-values larger than 0.999. The relative standard deviation of Cu^+ (324.752 nm) or In^{3+} (325.609 nm) concentration was less than 3%.

ASSOCIATED CONTENT

Supporting Information

The Supporting Information is available free of charge on the ACS Publications website at DOI: 10.1021/acsnano.8b03641.

XRD patterns of template $Cu_{2-x}S$ NCs and product CIS QDs; TEM images and corresponding size histograms of CIS QDs with a size range from 2.7 to 6.8 nm; PL spectra of product CIS QDs; detailed parameters for synthesizing CIS QDs *via* partial cation exchange in template Cu_{2-x}NCs; determination of CIS QD concentration; PL peak positions and second derivative of absorption spectra of 5.5 nm CIS QDs (PDF)

AUTHOR INFORMATION

Corresponding Author

*E-mail: c.demello-donega@uu.nl.

ORCID

Chenghui Xia: 0000-0001-5087-8805

Xiaobin Xie: 0000-0003-0190-1807

Celso de Mello Donega: 0000-0002-4403-3627

Notes

The authors declare no competing financial interest.

ACKNOWLEDGMENTS

C.X. acknowledges the China Scholarship Council (CSC) for financial support (no. 201406330055). X.X. acknowledges the financial support from the EU H2020-MSCA-ITN-2015 project "MULTIMAT" (project number: 676045). C.d.M.D. acknowledges financial support from the division of Chemical Sciences (CW) of The Netherlands Organization for Scientific

DOI: 10.1021/acsnano.8b03641
ACS Nano 2018, 12, 8350−8361

Research (NWO) under Grant Number ECHO.712.014.001. The authors thank G. Wang for XRD measurements.

REFERENCES

(1) Pietryga, J. M.; Park, Y. S.; Lim, J.; Fidler, A. F.; Bae, W. K.; Brovelli, S.; Klimov, V. I. Spectroscopic and Device Aspects of Nanocrystal Quantum Dots. *Chem. Rev.* **2016**, *116*, 10513−10622.

(2) Liu, M.; Voznyy, O.; Sabatini, R.; de Arquer, F. P. G.; Munir, R.; Balawi, A. H.; Lan, X.; Fan, F.; Walters, G.; Kirmani, A. R.; Hoogland, S.; Laquai, F.; Amassian, A.; Sargent, E. H. Hybrid Organic−Inorganic Inks Flatten the Energy Landscape in Colloidal Quantum Dot Solids. *Nat. Mater.* **2017**, *16*, 258−263.

(3) Kim, M. R.; Ma, D. Quantum-Dot-Based Solar Cells: Recent Advances, Strategies, and Challenges. *J. Phys. Chem. Lett.* **2015**, *6*, 85−99.

(4) de Arquer, F. P. G.; Armin, A.; Meredith, P.; Sargent, E. H. Solution-Processed Semiconductors for Next-Generation Photodetectors. *Nat. Rev. Mater.* **2017**, *2*, 16100.

(5) Panfil, Y. E.; Oded, M.; Banin, U. Colloidal Quantum Nanostructures: Emerging Materials for Display Applications. *Angew. Chem., Int. Ed.* **2018**, *57*, 2−24.

(6) Kagan, C. R.; Lifshitz, E.; Sargent, E. H.; Talapin, D. V. Building Devices from Colloidal Quantum Dots. *Science* **2016**, *353*, aac5523.

(7) Pelaz, B.; Alexiou, C.; Alvarez-Puebla, R. A.; Alves, F.; Andrews, A. M.; Ashraf, S.; Balogh, L. P.; Ballerini, L.; Bestetti, A.; Brendel, C.; Bosi, S.; Carril, M.; Chan, W. C. W.; Chen, C.; Chen, X.; Chen, X.; Cheng, Z.; Cui, D.; Du, J.; Dullin, C.; et al. Diverse Applications of Nanomedicine. *ACS Nano* **2017**, *11*, 2313−2381.

(8) Xu, G.; Zeng, S.; Zhang, B.; Swihart, M. T.; Yong, K. T.; Prasad, P. N. New Generation Cadmium-Free Quantum Dots for Biophotonics and Nanomedicine. *Chem. Rev.* **2016**, *116*, 12234−12327.

(9) Medintz, I. L.; Uyeda, H. T.; Goldman, E. R.; Mattoussi, H. Quantum Dot Bioconjugates for Imaging, Labelling and Sensing. *Nat. Mater.* **2005**, *4*, 435−446.

(10) Xia, C.; Winckelmans, N.; Prins, P. T.; Bals, S.; Gerritsen, H. C.; de Mello Donega, C. Near-Infrared-Emitting $CuInS_2$/ZnS Dot-in-Rod Colloidal Heteronanorods by Seeded Growth. *J. Am. Chem. Soc.* **2018**, *140*, 5755−5763.

(11) Zhou, J.; Zhu, M.; Meng, R.; Qin, H.; Peng, X. Ideal CdSe/CdS Core/Shell Nanocrystals Enabled by Entropic Ligands and Their Core Size-, Shell Thickness-, and Ligand-Dependent Photoluminescence Properties. *J. Am. Chem. Soc.* **2017**, *139*, 16556−16567.

(12) Donega, C. d. M. Synthesis and Properties of Colloidal Heteronanocrystals. *Chem. Soc. Rev.* **2011**, *40*, 1512−1546.

(13) van der Stam, W.; Rabouw, F. T.; Vonk, S. J. W.; Geuchies, J. J.; Ligthart, H.; Petukhov, A. V.; de Mello Donega, C. Oleic Acid-Induced Atomic Alignment of ZnS Polyhedral Nanocrystals. *Nano Lett.* **2016**, *16*, 2608−2614.

(14) Geuchies, J. J.; van Overbeek, C.; Evers, W. H.; Goris, B.; de Backer, A.; Gantapara, A. P.; Rabouw, F. T.; Hilhorst, J.; Peters, J. L.; Konovalov, O.; Petukhov, A. V.; Dijkstra, M.; Siebbeles, L. D. A.; van Aert, S.; Bals, S.; Vanmaekelbergh, D. *In Situ* Study of the Formation Mechanism of Two-Dimensional Superlattices from PbSe Nanocrystals. *Nat. Mater.* **2016**, *15*, 1248−1254.

(15) Boles, M. A.; Engel, M.; Talapin, D. V. Self-Assembly of Colloidal Nanocrystals: From Intricate Structures to Functional Materials. *Chem. Rev.* **2016**, *116*, 11220−11289.

(16) Thanh, N. T. K.; Maclean, N.; Mahiddine, S. Mechanisms of Nucleation and Growth of Nanoparticles in Solution. *Chem. Rev.* **2014**, *114*, 7610−7630.

(17) Angeloni, I.; Raja, W.; Brescia, R.; Polovitsyn, A.; De Donato, F.; Canepa, M.; Bertoni, G.; Zaccaria, R. P.; Moreels, I. Disentangling the Role of Shape, Ligands, and Dielectric Constants in the Absorption Properties of Colloidal CdSe/CdS Nanocrystals. *ACS Photonics* **2016**, *3*, 58−67.

(18) Langevin, M. A.; Lachance-Quirion, D.; Ritcey, A. M.; Allen, C. N. Size-Dependent Extinction Coefficients and Transition Energies of Near-Infrared β-Ag_2Se Colloidal Quantum Dots. *J. Phys. Chem. C* **2013**, *117*, 5424−5428.

(19) Gong, K.; Zeng, Y.; Kelley, D. F. Extinction Coefficients, Oscillator Strengths, and Radiative Lifetimes of CdSe, CdTe, and CdTe/CdSe Nanocrystals. *J. Phys. Chem. C* **2013**, *117*, 20268−20279.

(20) Yang, C. C.; Mai, Y. W. Size-Dependent Absorption Properties of CdX (X= S, Se, Te) Quantum Dots. *Chem. Phys. Lett.* **2012**, *535*, 91−93.

(21) Čapek, R. K.; Moreels, I.; Lambert, K.; De Muynck, D.; Zhao, Q.; Van Tomme, A.; Vanhaecke, F.; Hens, Z. Optical Properties of Zincblende Cadmium Selenide Quantum Dots. *J. Phys. Chem. C* **2010**, *114*, 6371−6376.

(22) Dong, C.; Ren, J. Measurements for Molar Extinction Coefficients of Aqueous Quantum Dots. *Analyst* **2010**, *135*, 1395−1399.

(23) Moreels, I.; Lambert, K.; Smeets, D.; De Muynck, D.; Nollet, T.; Martins, J. C.; Vanhaecke, F.; Vantomme, A.; Delerue, C.; Allan, G.; Hens, Z. Size-Dependent Optical Properties of Colloidal PbS Quantum Dots. *ACS Nano* **2009**, *3*, 3023−3030.

(24) Jasieniak, J.; Smith, L.; van Embden, J.; Mulvaney, P.; Califano, M. Re-Examination of the Size-Dependent Absorption Properties of CdSe Quantum Dots. *J. Phys. Chem. C* **2009**, *113*, 19468−19474.

(25) Donega, C. d. M.; Koole, R. Size Dependence of the Spontaneous Emission Rate and Absorption Cross Section of CdSe and CdTe Quantum Dots. *J. Phys. Chem. C* **2009**, *113*, 6511−6520.

(26) Dai, Q.; Wang, Y.; Li, X.; Zhang, Y.; Pellegrino, D. J.; Zhao, M.; Zou, B.; Seo, J.; Wang, Y.; Yu, W. W. Size-Dependent Composition and Molar Extinction Coefficient of PbSe Semiconductor Nanocrystals. *ACS Nano* **2009**, *3*, 1518−1524.

(27) Sun, J.; Goldys, E. M. Linear Absorption and Molar Extinction Coefficients in Direct Semiconductor Quantum Dots. *J. Phys. Chem. C* **2008**, *112*, 9261−9266.

(28) Moreels, I.; Lambert, K.; De Muynck, D.; Vanhaecke, F.; Poelman, D.; Martins, J. C.; Allan, G.; Hens, Z. Composition and Size-Dependent Extinction Coefficient of Colloidal PbSe Quantum Dots. *Chem. Mater.* **2007**, *19*, 6101−6106.

(29) Protasenko, V.; Bacinello, D.; Kuno, M. Experimental Determination of the Absorption Cross-Section and Molar Extinction Coefficient of CdSe and CdTe Nanowires. *J. Phys. Chem. B* **2006**, *110*, 25322−25331.

(30) Cademartiri, L.; Montanari, E.; Calestani, G.; Migliori, A.; Guagliardi, A.; Ozin, G. A. Size-Dependent Extinction Coefficients of PbS Quantum Dots. *J. Am. Chem. Soc.* **2006**, *128*, 10337−10346.

(31) Yu, W. W.; Qu, L.; Guo, W.; Peng, X. Experimental Determination of the Extinction Coefficient of CdTe, CdSe, and CdS Nanocrystals. *Chem. Mater.* **2003**, *15*, 2854−2860.

(32) Striolo, A.; Ward, J.; Prausnitz, J. M.; Parak, W. J.; Zanchet, D.; Gerion, D.; Milliron, D.; Alivisatos, A. P. Molecular Weight, Osmotic Second Virial Coefficient, and Extinction Coefficient of Colloidal CdSe Nanocrystals. *J. Phys. Chem. B* **2002**, *106*, 5500−5505.

(33) Leatherdale, C. A.; Woo, W. K.; Mikulec, F. V.; Bawendi, M. G. On the Absorption Cross Section of CdSe Nanocrystal Quantum Dots. *J. Phys. Chem. B* **2002**, *106*, 7619−7622.

(34) Schmelz, O.; Mews, A.; Basché, T.; Herrmann, A.; Müllen, K. Supramolecular Complexes from CdSe Nanocrystals and Organic Fluorophors. *Langmuir* **2001**, *17*, 2861−2865.

(35) Vossmeyer, T.; Katsikas, L.; Giersig, M.; Popovic, I. G.; Diesner, K.; Chemseddine, A.; Eychmueller, A.; Weller, H. CdS Nanoclusters: Synthesis, Characterization, Size Dependent Oscillator Strength, Temperature Shift of the Excitonic Transition Energy, and Reversible Absorbance Shift. *J. Phys. Chem.* **1994**, *98*, 7665−7673.

(36) Talapin, D. V.; Gaponik, N.; Borchert, H.; Rogach, A. L.; Haase, M.; Weller, H. Etching of Colloidal InP Nanocrystals with Fluorides: Photochemical Nature of the Process Resulting in High Photoluminescence Efficiency. *J. Phys. Chem. B* **2002**, *106*, 12659−12663.

(37) Xie, R.; Peng, X. Synthetic Scheme for High-Quality InAs Nanocrystals Based on Self-Focusing and One-Pot Synthesis of InAs-

DOI: 10.1021/acsnano.8b03641
ACS Nano 2018, 12, 8350−8361

Based Core-Shell Nanocrystals. *Angew. Chem., Int. Ed.* **2008**, *47*, 7677−7680.
(38) Yu, P.; Beard, M. C.; Ellingson, R. J.; Ferrere, S.; Curtis, C.; Drexler, J.; Luiszer, F.; Nozik, A. J. Absorption Cross-Section and Related Optical Properties of Colloidal InAs Quantum Dots. *J. Phys. Chem. B* **2005**, *109*, 7084−7087.
(39) Coughlan, C.; Ibáñez, M.; Dobrozhan, O.; Singh, A.; Cabot, A.; Ryan, K. M. Compound Copper Chalcogenide Nanocrystals. *Chem. Rev.* **2017**, *117*, 5865−6109.
(40) van der Stam, W.; Berends, A. C.; de Mello Donega, C. Prospects of Colloidal Copper Chalcogenide Nanocrystals. *ChemPhysChem* **2016**, *17*, 559−581.
(41) Kolny-Olesiak, J.; Weller, H. Synthesis and Application of Colloidal $CuInS_2$ Semiconductor Nanocrystals. *ACS Appl. Mater. Interfaces* **2013**, *5*, 12221−12237.
(42) Chen, B.; Pradhan, N.; Zhong, H. From Large-Scale Synthesis to Lighting Device Applications of Ternary I−III−VI Semiconductor Nanocrystals: Inspiring Greener Material Emitters. *J. Phys. Chem. Lett.* **2018**, *9*, 435−445.
(43) Wepfer, S.; Frohleiks, J.; Hong, A. R.; Jang, H. S.; Bacher, G.; Nannen, E. Solution-Processed $CuInS_2$-Based White QD-LEDs with Mixed Active Layer Architecture. *ACS Appl. Mater. Interfaces* **2017**, *9*, 11224−11230.
(44) Chuang, P. H.; Lin, C. C.; Liu, R. S. Emission-Tunable $CuInS_2$/ZnS Quantum Dots: Structure, Optical Properties, and Application in White Light-Emitting Diodes with High Color Rendering Index. *ACS Appl. Mater. Interfaces* **2014**, *6*, 15379−15387.
(45) Wu, K.; Li, H.; Klimov, V. I. Tandem Luminescent Solar Concentrators Based on Engineered Quantum Dots. *Nat. Photonics* **2018**, *12*, 105−110.
(46) Meinardi, F.; McDaniel, H.; Carulli, F.; Colombo, A.; Velizhanin, K. A.; Makarov, N. S.; Simonutti, R.; Klimov, V. I.; Brovelli, S. Highly Efficient Large-Area Colourless Luminescent Solar Concentrators Using Heavy-Metal-Free Colloidal Quantum Dots. *Nat. Nanotechnol.* **2015**, *10*, 878−885.
(47) Knowles, K. E.; Kilburn, T. B.; Alzate, D. G.; McDowall, S.; Gamelin, D. R. Bright $CuInS_2$/CdS Nanocrystal Phosphors for High-Gain Full-Spectrum Luminescent Solar Concentrators. *Chem. Commun.* **2015**, *51*, 9129−9132.
(48) Bergren, M. R.; Makarov, N. S.; Ramasamy, K.; Jackson, A.; Guglielmetti, R.; McDaniel, H. High-Performance $CuInS_2$ Quantum Dot Laminated Glass Luminescent Solar Concentrators for Windows. *ACS Energy Letters* **2018**, *3*, 520−525.
(49) Yang, Y.; Lin, L.; Jing, L.; Yue, X.; Dai, Z. $CuInS_2$/ZnS Quantum Dots Conjugating Gd(3+) Chelates for Near-Infrared Fluorescence and Magnetic Resonance Bimodal Imaging. *ACS Appl. Mater. Interfaces* **2017**, *9*, 23450−23457.
(50) Pons, T.; Pic, E.; Lequeux, N.; Cassette, E.; Bezdetnaya, L.; Guillemin, F.; Marchal, F.; Dubertret, B. Cadmium-Free $CuInS_2$/ZnS Quantum Dots for Sentinel Lymph Node Imaging with Reduced Toxicity. *ACS Nano* **2010**, *4*, 2531−2538.
(51) Qin, L.; Li, D.; Zhang, Z.; Wang, K.; Ding, H.; Xie, R.; Yang, W. The Determination of Extinction Coefficient of $CuInS_2$, and $ZnCuInS_3$ Multinary Nanocrystals. *Nanoscale* **2012**, *4*, 6360−6364.
(52) Booth, M.; Brown, A. P.; Evans, S. D.; Critchley, K. Determining the Concentration of $CuInS_2$ Quantum Dots from the Size-Dependent Molar Extinction Coefficient. *Chem. Mater.* **2012**, *24*, 2064−2070.
(53) Berends, A. C.; van der Stam, W.; Hofmann, J. P.; Bladt, E.; Meeldijk, J. D.; Bals, S.; de Mello Donega, C. Interplay between Surface Chemistry, Precursor Reactivity, and Temperature Determines Outcome of ZnS Shelling Reactions on $CuInS_2$ Nanocrystals. *Chem. Mater.* **2018**, *30*, 2400−2413.
(54) Berends, A. C.; Rabouw, F. T.; Spoor, F. C. M.; Bladt, E.; Grozema, F. C.; Houtepen, A. J.; Siebbeles, L. D. A.; de Mello Donega, C. Radiative and Nonradiative Recombination in $CuInS_2$ Nanocrystals and $CuInS_2$-Based Core/Shell Nanocrystals. *J. Phys. Chem. Lett.* **2016**, *7*, 3503−3509.
(55) Zhong, H.; Lo, S. S.; Mirkovic, T.; Li, Y.; Ding, Y.; Li, Y.; Scholes, G. D. Noninjection Gram-Scale Synthesis of Monodisperse Pyramidal $CuInS_2$ Nanocrystals and Their Size-Dependent Properties. *ACS Nano* **2010**, *4*, 5253−5262.
(56) Akdas, T.; Walter, J.; Segets, D.; Distaso, M.; Winter, B.; Birajdar, B.; Spiecker, E.; Peukert, W. Investigation of the Size-Property Relationship in $CuInS_2$ Quantum Dots. *Nanoscale* **2015**, *7*, 18105−18118.
(57) Li, L.; Pandey, A.; Werder, D. J.; Khanal, B. P.; Pietryga, J. M.; Klimov, V. I. Efficient Synthesis of Highly Luminescent Copper Indium Sulfide-Based Core/Shell Nanocrystals with Surprisingly Long-Lived Emission. *J. Am. Chem. Soc.* **2011**, *133*, 1176−1179.
(58) Xia, C.; Meeldijk, J. D.; Gerritsen, H. C.; de Mello Donega, C. Highly Luminescent Water-Dispersible NIR-Emitting Wurtzite $CuInS_2$/ZnS Core/Shell Colloidal Quantum Dots. *Chem. Mater.* **2017**, *29*, 4940−4951.
(59) van der Stam, W.; Berends, A. C.; Rabouw, F. T.; Willhammar, T.; Ke, X.; Meeldijk, J. D.; Bals, S.; de Mello Donega, C. Luminescent $CuInS_2$ Quantum Dots by Partial Cation Exchange in $Cu_{2-x}S$ Nanocrystals. *Chem. Mater.* **2015**, *27*, 621−628.
(60) Qi, Y.; Liu, Q.; Tang, K.; Liang, Z.; Ren, Z.; Liu, X. Synthesis and Characterization of Nanostructured Wurtzite $CuInS_2$: A New Cation Disordered Polymorph of $CuInS_2$. *J. Phys. Chem. C* **2009**, *113*, 3939−3944.
(61) Xia, C.; Cao, L.; Liu, W.; Su, G.; Gao, R.; Qu, H.; Shi, L.; He, G. One-Step Synthesis of Near-Infrared Emitting and Size Tunable $CuInS_2$ Semiconductor Nanocrystals by Adjusting Kinetic Variables. *CrystEngComm* **2014**, *16*, 7469−7477.
(62) Shi, Y.; Jin, Z.; Li, C.; An, H.; Qiu, J. Effect of [Cu]/[In] Ratio on Properties of $CuInS_2$ Thin Films Prepared by Successive Ionic Layer Absorption and Reaction Method. *Appl. Surf. Sci.* **2006**, *252*, 3737−3743.
(63) Guillén, C.; Herrero, J. $CuInS_2$ and $CuGaS_2$ Thin Films Grown by Modulated Flux Deposition with Various Cu Contents. *Phys. Status Solidi A* **2006**, *203*, 2438−2443.
(64) Zhang, S. B.; Wei, S. H.; Zunger, A.; Katayama-Yoshida, H. Defect Physics of the $CuInSe_2$ Chalcopyrite Semiconductor. *Phys. Rev. B: Condens. Matter Mater. Phys.* **1998**, *57*, 9642−9656.
(65) Ueng, H. Y.; Hwang, H. L. The Defect Structure of $CuInS_2$. Part I: Intrinsic Defects. *J. Phys. Chem. Solids* **1989**, *50*, 1297−1305.
(66) Jaffe, J. E.; Zunger, A. Electronic Structure of the Ternary Chalcopyrite Semiconductors $CuAlS_2$, $CuGaS_2$, $CuInS_2$, $CuAlSe_2$, $CuGaSe_2$, and $CuInSe_2$. *Phys. Rev. B: Condens. Matter Mater. Phys.* **1983**, *28*, 5822−5847.
(67) Chen, B.; Zhong, H.; Zhang, W.; Tan, Z. A.; Li, Y.; Yu, C.; Zhai, T.; Bando, Y.; Yang, S.; Zou, B. Highly Emissive and Color-Tunable $CuInS_2$-Based Colloidal Semiconductor Nanocrystals: Off-Stoichiometry Effects and Improved Electroluminescence Performance. *Adv. Funct. Mater.* **2012**, *22*, 2081−2088.
(68) Leach, A. D. P.; Macdonald, J. E. Optoelectronic Properties of $CuInS_2$ Nanocrystals and Their Origin. *J. Phys. Chem. Lett.* **2016**, *7*, 572−583.
(69) Donega, C. d. M. Formation of Nanoscale Spatially Indirect Excitons: Evolution of the Type-II Optical Character of CdTe/CdSe Heteronanocrystals. *Phys. Rev. B: Condens. Matter Mater. Phys.* **2010**, *81*, 165303.
(70) Liptay, T. J.; Marshall, L. F.; Rao, P. S.; Ram, R. J.; Bawendi, M. G. Anomalous Stokes Shift in CdSe Nanocrystals. *Phys. Rev. B: Condens. Matter Mater. Phys.* **2007**, *76*, 155314.
(71) Pinchetti, V.; Lorenzon, M.; McDaniel, H.; Lorenzi, R.; Meinardi, F.; Klimov, V. I.; Brovelli, S. Spectro-Electrochemical Probing of Intrinsic and Extrinsic Processes in Exciton Recombination in $I-III-VI_2$ Nanocrystals. *Nano Lett.* **2017**, *17*, 4508−4517.
(72) Fuhr, A. S.; Yun, H. J.; Makarov, N. S.; Li, H.; McDaniel, H.; Klimov, V. I. Light Emission Mechanisms in $CuInS_2$ Quantum Dots Evaluated by Spectral Electrochemistry. *ACS Photonics* **2017**, *4*, 2425−2435.
(73) Knowles, K. E.; Hartstein, K. H.; Kilburn, T. B.; Marchioro, A.; Nelson, H. D.; Whitham, P. J.; Gamelin, D. R. Luminescent Colloidal

DOI: 10.1021/acsnano.8b03641
ACS Nano 2018, 12, 8350−8361

Semiconductor Nanocrystals Containing Copper: Synthesis, Photophysics, and Applications. *Chem. Rev.* **2016**, *116*, 10820−10851.
(74) Koole, R.; Allan, G.; Delerue, C.; Meijerink, A.; Vanmaekelbergh, D.; Houtepen, A. J. Optical Investigation of Quantum Confinement in PbSe Nanocrystals at Different Points in the Brillouin Zone. *Small* **2008**, *4*, 127−133.
(75) Shabaev, A.; Mehl, M. J.; Efros, A. L. Energy Band Structure of $CuInS_2$ and Optical Spectra of $CuInS_2$ Nanocrystals. *Phys. Rev. B: Condens. Matter Mater. Phys.* **2015**, *92*, 035431.
(76) Allan, G.; Delerue, C. Confinement Effects in PbSe Quantum Wells and Nanocrystals. *Phys. Rev. B: Condens. Matter Mater. Phys.* **2004**, *70*, 245321.
(77) Tomić, S.; Bernasconi, L.; Searle, B. G.; Harrison, N. M. Electronic and Optical Structure of Wurtzite $CuInS_2$. *J. Phys. Chem. C* **2014**, *118*, 14478−14484.
(78) Huang, W. C.; Tseng, C. H.; Chang, S. H.; Tuan, H. Y.; Chiang, C. C.; Lyu, L. M.; Huang, M. H. Solvothermal Synthesis of Zincblende and Wurtzite $CuInS_2$ Nanocrystals and Their Photovoltaic Application. *Langmuir* **2012**, *28*, 8496−8501.
(79) Alonso, M. I.; Wakita, K.; Pascual, J.; Garriga, M.; Yamamoto, N. Optical Functions and Electronic Structure of $CuInSe_2$, $CuGaSe_2$, $CuInS_2$, and $CuGaS_2$. *Phys. Rev. B: Condens. Matter Mater. Phys.* **2001**, *63*, 075203.
(80) Brus, L. E. Electron−Electron and Electron−Hole Interactions in Small Semiconductor Crystallites: The Size Dependence of the Lowest Excited Electronic State. *J. Chem. Phys.* **1984**, *80*, 4403−4409.
(81) Mudryi, A. V.; Yakushev, M. V.; Volkov, V. A.; Zhivulko, V. D.; Borodavchenko, O. M.; Martin, R. W. Influence of the Growth Method on the Photoluminescence Spectra and Electronic Properties of $CuInS_2$ Single Crystals. *J. Lumin.* **2017**, *186*, 123−126.
(82) Omata, T.; Nose, K.; Otsuka-Yao-Matsuo, S. Size Dependent Optical Band Gap of Ternary I-III-VI_2 Semiconductor Nanocrystals. *J. Appl. Phys.* **2009**, *105*, 073106.
(83) Efros, A. L.; Rosen, M.; Kuno, M.; Nirmal, M.; Norris, D. J.; Bawendi, M. Band-Edge Exciton in Quantum Dots of Semiconductors with a Degenerate Valence Band: Dark and Bright Exciton States. *Phys. Rev. B: Condens. Matter Mater. Phys.* **1996**, *54*, 4843−4856.
(84) Ramaniah, L. M.; Nair, S. V. Optical Absorption in Semiconductor Quantum Dots: a Tight-Binding Approach. *Phys. Rev. B: Condens. Matter Mater. Phys.* **1993**, *47*, 7132−7139.
(85) Laheld, U. E. H.; Einevoll, G. T. Excitons in CdSe Quantum Dots. *Phys. Rev. B: Condens. Matter Mater. Phys.* **1997**, *55*, 5184−5204.
(86) Rajh, T.; Mićić, O. I.; Nozik, A. J. Synthesis and Characterization of Surface-Modified Colloidal CdTe Quantum Dots. *J. Phys. Chem.* **1993**, *97*, 11999−12003.
(87) Klimov, V. I. Optical Nonlinearities and Ultrafast Carrier Dynamics in Semiconductor Nanocrystals. *J. Phys. Chem. B* **2000**, *104*, 6112−6123.
(88) Ricard, D.; Ghanassi, M.; Schanne-Klein, M. C. Dielectric Confinement and the Linear and Nonlinear Optical Properties of Semiconductor-Doped Glasses. *Opt. Commun.* **1994**, *108*, 311−318.
(89) Gao, B.; Tang, F. L.; Xue, H. T.; Zhang, F. Z.; Cheng, Y. W. Configuration Dependent Electronic and Optical Properties of WZ-$CuInS_2$. *Am. J. Opt. Photonics* **2016**, *4*, 32−39.
(90) Levcenko, S.; Syrbu, N. N.; Tezlevan, V. E.; Arushanov, E.; Doka-Yamigno, S.; Schedel-Niedrig, T.; Lux-Steiner, M. C. Optical Spectra and Energy Band Structure of Single Crystalline $CuGaS_2$ and $CuInS_2$. *J. Phys.: Condens. Matter* **2007**, *19*, 456222.
(91) Benson, R. C.; Kues, H. A. Fluorescence Properties of Indocyanine Green as Related to Angiography. *Phys. Med. Biol.* **1978**, *23*, 159−163.

DOI: 10.1021/acsnano.8b03641
ACS Nano 2018, 12, 8350−8361